International Journal of Heat and Mass Transfer 52 (2009) 3534–3546

Contents lists available at ScienceDirect

International Journal of Heat and Mass Transfer

journal homepage: www.elsevier.com/locate/ijhmt

Wall heat flux partitioning during subcooled forced flow film boiling of water on a vertical surface

Phani K. Meduri, Gopinath R. Warrier, Vijay K. Dhir *

Mechanical and Aerospace Engineering Department, Henri Samueli School of Engineering and Applied Science, University of California, Los Angeles, CA 90095, USA

ARTICLE INFO

Article history:
Received 29 February 2008
Received in revised form 13 February 2009
Accepted 13 February 2009
Available online 23 April 2009

Keywords:
Subcooled flow film boiling
Wall heat flux partitioning

ABSTRACT

Subcooled flow film boiling experiments were conducted on a vertical flat plate, 30.5 cm in height, and 3.175 cm wide with forced convective upflow of subcooled water at atmospheric pressure. Data have been obtained for mass fluxes ranging from 0 to 700 kg/m^{2}s, inlet subcoolings ranging from 0 to 25 °C and wall superheats ranging from 200 to 400 °C. Correlations for wall heat transfer coefficient and wall heat flux partitioning were developed as part of this work. These correlations derive their support from simultaneous measurements of the wall heat flux, fluid temperature profiles, liquid side heat flux and interfacial wave behavior during steady state flow film boiling. A new correlation for the film collapse temperature was also deduced by considering the limiting case of heat flux to the subcooled liquid being equal to the wall heat flux. The premise of this deduction is that film collapse under subcooled conditions occurs when there is no net vapor generation. These correlations have also been compared with the data and correlations available in the literature.

1. Introduction

Understanding the heat transfer processes during film boiling is important in many areas of engineering technology and geophysics such as nuclear safety, cooling of rocket engines, quenching of metals and flow of cryogenic liquids in heated pipes. At relatively high flooding rates, when the wall temperature is too high for the liquid to rewet the wall, and particularly if the liquid at the axially progressing quench front is subcooled, a liquid column is formed downstream of the quench front, separated from the hot wall by a thin vapor film. The vapor film can accommodate steep velocity and temperature gradients. This flow regime is known as inverted annular film boiling. Inverse annular flow film boiling typically involves heat transfer from the wall to the vapor blanket and subsequently from the vapor to the liquid core. Some heat will also be transferred directly from the wall to the liquid core by radiation. Many experimental and theoretical studies have been conducted to quantify the heat transfer during film boiling, some of which are discussed below.

Since Bromley's [1] study of film boiling, numerous analytical/numerical [2–5] and experimental [5–8] studies of saturated and subcooled film boiling on heaters of various geometries have appeared in the literature. An extensive review of the previous work is given in [9] and [10]. In general it is observed that the results of analytical and numerical work, in which a stable laminar film with a smooth vapor–liquid interface is assumed, agree with the experimental results only close to the quench front. Further downstream of the quench front, these analyses tend to under-predict the average heat transfer coefficient and inaccurately predict the dependence of the local heat transfer coefficient on the distance from the leading edge. From the visual observations of vapor–liquid interface during film boiling [7,8], it was observed that the vapor–liquid interface is covered by waves of different wavelengths. A smooth interface exists only a short distance near the leading edge.

Greitzer and Abernathy [6] recognized the importance of the presence of bulges of vapor at the vapor–liquid interface to the film boiling heat transfer mechanism and presented a model for film boiling in which the time dependence of the phenomenon is taken into account. Using mechanistic arguments, they were able to relate relevant terms representing the total force exerted by the vapor on the mass of liquid adjacent to the vapor film and the buoyancy and drag forces on the bubbles to the bubble size and velocity and were thereby able to obtain an expression for the average heat transfer coefficient. Their expression however, under-predicts experimental data for Freon-113 by a factor of three to four and does not accurately predict the variation of heat transfer coefficient with heater length.

Noting that the heat transfer coefficients predicted by laminar models were lower than the experimental data, several investigators [11–13] argued that the vapor flow in the film must be turbulent after short distances from the leading edge. These models based on turbulent flow however predict significantly lower heat transfer coefficients than the experimentally determined values. For common fluids boiling on vertical surfaces of the length of

* Corresponding author. Tel.: +1 310 825 9617; fax: +1 310 206 4830.
E-mail address: vdhir@seas.ucla.edu (V.K. Dhir).

0017-9310/$ - see front matter © 2009 Published by Elsevier Ltd.
doi:10.1016/j.ijheatmasstransfer.2009.02.040

Nomenclature

C_p	specific heat
h	heat transfer coefficient
h_{fg}	latent heat of vaporization
g	acceleration due to gravity
G	mass flux
Ja	Jacob number $\left(Ja_{sub}=\frac{C_{Pl}\Delta T_{sub}}{h_{fg}}, Ja_{sup}=\frac{C_{Pv}\Delta T_w}{h_{fg}}\right)$
k	thermal conductivity
l_{waves}	distance required for the formation of the waves as measured from the leading edge
L_c	characteristic length scale $\left(L_c=\sqrt{\frac{\sigma}{g(\rho_l-\rho_v}}\right)$
l^*	dimensionless distance for the formation of waves $\left(l^*=\frac{l_{waves}}{L_c}\right)$
Nu	Nusselt Number $\left(Nu=\frac{hL_c}{k_v}\right)$
P	pressure
Pr	Prandtl number
q	heat flux
Re	Reynolds number $\left(Re=\frac{\rho UL_c}{\mu}\right)$
T	temperature
U	velocity
y	distance normal to the heater surface
z	axial distance from the leading edge
z^*	dimensionless axial distance $\left(z^*=\frac{Z}{L_c}\right)$
ΔT	temperature difference

Greek letters

δ	vapor film thickness
μ	viscosity
ρ	density
σ	surface tension

Subscripts

conv	convective
cr	critical
fc	film collapse
i	interface
i–l	vapor–liquid interface to liquid
in	inlet
l	liquid
MFB	minimum film boiling
sub	subcooling
sup	superheat
sat	saturated
v	vapor
w	wall

ten centimetres or so, the vapor film Reynolds number is certainly not high enough to justify the assumption of a turbulent vapor film. Turbulent vapor flow if it exists is produced by time-dependent wave oscillation. This turbulent flow will be confined to the region under large amplitude waves. However, Bui and Dhir [7] showed that the contribution of the region under large amplitude waves to the overall heat transfer rate is small.

Bui and Dhir [7] studied saturated pool film boiling on a vertical flat plate. Their study involved both experiments and mechanistic modeling. Their model assumed that as the vapor flow path becomes longer with increasing surface length, the vapor–liquid interface becomes unstable and interfacial waves are formed. The peaks of the waves appear as bulges. By dividing the vapor film into cells supporting a single bulge, the film boiling heat transfer coefficients are obtained for each cell. Their model was found to compare well with experimental heat transfer coefficients for saturated film boiling on a vertical flat plate.

Vijaykumar and Dhir [8] extended the work of Bui and Dhir [7] and studied natural convection film boiling of subcooled water. They showed from their experiments that the existing theoretical models for subcooled film boiling are insufficient and that to understand and predict subcooled film boiling accurately, one has to consider the vapor–liquid interface behavior in great detail. Using still photography and video pictures, they observed the existence of a finite vapor layer at the leading edge and ripples and large waves (bubbles) on the interface. The interface and liquid velocities in the boundary layer adjacent to the interface were measured using hydrogen bubble flow visualization method and the liquid side heat flux was measured using holographic interferometry. They also developed theoretical models for the wavelength and the interfacial velocity. However, they did not develop any model for wall heat transfer including the effect of interfacial waves.

Aritomi et al. [14] conducted inverted annular film boiling experiments under various heat flux, inlet velocity and inlet subcooling conditions using Freon-113. They proposed empirical correlations for net vaporization rate from the interface, heat flux from the interface to the liquid phase, interfacial shear stress and heat transfer coefficient from the wall to the liquid. However, these correlations all have the vapor film thickness as one of the parameters and the film thickness being an unknown in most situations renders these correlations not very useful for prediction. Also, no direct measurements of the interfacial heat transfer were made in this experimental work. Comparisons of the correlations were made only against the measured wall heat transfer coefficient.

Because of the large amount of empiricism built in the previous models, all the deviations between the experimental data and the model predictions are concealed in the empirical constants. The errors arising out of various approximations made while developing these models will be masked by these approaches because ultimately it is only the total heat transfer coefficient which was compared with the data and not the individual parameters like the vapor film thickness or the interfacial heat transfer.

In order to develop a mechanistic model for the subcooled flow film boiling process, the key issues that need to be addressed are wall heat flux partitioning and interfacial heat transfer. The pool film boiling data given in [8] is the only data available so far on liquid side heat transfer. Thus one of the goals of this study was to determine the rate of interfacial heat transfer that occurs during subcooled film boiling. The experimental data gathered during this study was used to expand the experimental database and develop relevant correlations. In addition a correlation for the minimum film collapse temperature was also deduced by considering the limiting condition where all the wall heat flux is utilized in heating up the liquid. This correlation is compared with existing models and experimental data.

2. Experimental apparatus and procedure

2.1. Experimental apparatus

The schematic of the flow loop is shown in Fig. 1(a). The flow loop consists of two tanks, each with a volume of 1.25 m^3, a centrifugal pump, turbine flow meter, bypass line, preheater and test

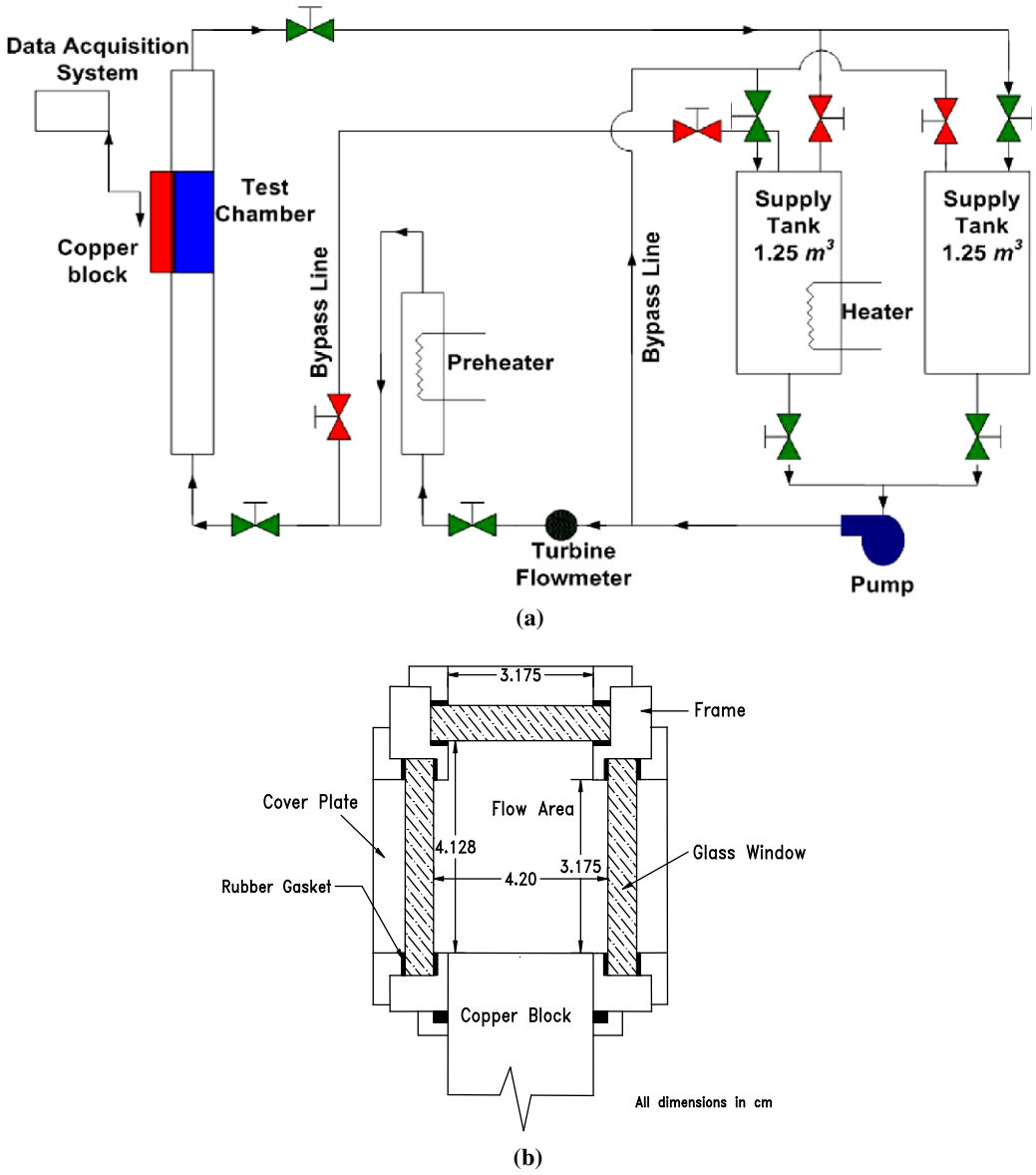

Fig. 1. (a) Schematic of the flow loop and (b) cross-section of the test chamber.

section. One of the supply tanks is also fitted with immersion heaters to degas and preheat the distilled water used in the experiments. The preheater consisted of a 210 kW flanged immersion heater fitted vertically onto a stainless steel container. The power to the immersion heater is controlled using a SCR power controller. Using the power controller and thermocouple outputs, it is possible to control the liquid subcooling accurately. Thermocouples and pressure transducers are installed at the inlet and exit of the heating section.

The flow channel for the test section is 1.83 m long, of which the heated section is 0.305 m. A 0.61 m long flow development section is provided upstream of the heated section, while a 0.305 m long section is provided downstream of the heated section. In addition, transition sections from circular to rectangular geometry, each 0.305 m long, are provided upstream and downstream of the test section. A flow straighter is also placed at the inlet of the flow developing section. The cross section of the flow channel is shown in Fig. 1(b). The flow channel is almost square in cross section with a flow area of 16.33 cm^2. The copper block, which is heated, is mounted flush with one of the inside walls of the flow channel, while pyrex glass windows are provided on the other three sides of the channel. The glass windows help in visual observation of the flow. The copper block has thermocouple embedded in them which are used to determine the temperature and heat flux at the surface. The thermocouples (K-type, 0.81 mm diameter) are located at seven different axial locations along the length of the copper block. At each axial location, there are eight thermocouples embedded in the block at discrete locations normal to the heating surface. Thus, a total of 56 thermocouples are placed in the copper block. The heating of the copper block is achieved using 36 cartridge heaters embedded in the back of the copper block. These cartridge heaters were arranged such that the heat flux at the boiling surface is uniform. The total installed power in the test section is 27 kW. The power supplied to the cartridge heaters, and hence to the copper block, is controlled with a SCR power controller.

Five microthermocouples (K-type, 0.25 mm diameter) are mounted in the test chamber to measure the liquid temperature profile adjacent to the test surface. These microthermocouples are connected to micrometers making it possible to traverse the width of the channel. They are used to measure liquid and vapor

temperatures at axial distances of 0.64 cm, 6.48 cm, 15.25 cm, 24.00 cm and 29.86 cm, respectively, from the leading edge of the copper surface.

2.2. Experimental procedure

Prior to each test run, the test surface was prepared as follows: (i) the surface was polished with 600 grit emery paper and then cleaned with DI water, (ii) the surface was then polished to a mirror finish using a metal polishing compound and then cleaned with acetone and DI water. Startup of a typical experiment began with degassing of the test liquid by vigorous boiling of the liquid as it passes over the preheater and through the bypass loop. The flow rate was then set to the required value. The flowrate was measured using the turbine flowmeter. Desired subcooling was maintained throughout the experimental run by controlling power to the preheater. The subcooling of the liquid could be maintained to within ±0.2 °C. Once the desired subcooling of the liquid was attained, the power to the cartridge heaters in the copper block was turned on. Initially, when the power supplied was low, the primary mechanism of heat transfer into the liquid was forced convection. The power was then gradually increased until transition from nucleate to film boiling was achieved. The power supply was then adjusted to attain the desired wall temperature. When steady state was reached, the temperatures were recorded on an Omega data acquisition system. Tests were considered to be at steady state when the temperature of the copper block changed by less than ±1 °C in five minutes. The vapor and the liquid temperature profiles were measured using traversable microthermocouples. The traversable microthermocouples were first moved in towards the heater surface till they just touch the surface and then they were moved out in steps of 0.025 mm till they measure the bulk liquid temperature. As they were being moved out, temperatures were recorded using a Personal DAQ (data acquisition) module.

Still and motion pictures of the interfacial wave structure were taken using a high-speed CCD camera. This camera is capable of recording pictures with a resolution of 256 × 256 pixels and has a maximum frame rate of 1220 frames/s. This camera is also capable of being fitted with lenses of various focal lengths as per experimental requirements.

2.3. Data reduction

Since the experiments were conducted under steady state conditions, the wall heat flux, q_w, was directly estimated from the temperature gradient measured with the thermocouples embedded in the copper block. The total power supplied to the copper block was also measured. A comparison of the measured and calculated total power shows that the difference is approximately 12% which means that the heat loss from the copper block was of the order of 12%. These losses are due to conduction to the stainless steel frame from the sides and the ends of the copper block. These losses were accounted for by assuming the heat transfer from the copper block to the stainless steel frame to be heat transfer to a semi-infinite solid. The details are given in [15]. The wall temperature, T_w was estimated by extrapolating these temperatures to the surface. The film boiling heat transfer coefficient (h_w) was then estimated as,

$$h_w(z) = \frac{q_w(z)}{(T_w(z) - T_{sat})} \tag{1}$$

Wall heat flux (q_w) was also estimated from the vapor temperature profiles by calculating the temperature gradient in the vapor film.

$$q_{w-v}(z) = -k_v \frac{\partial T}{\partial y}(z)\bigg|_w \tag{2}$$

Liquid side temperature gradient was estimated by calculating the gradient at the vapor–liquid interface of a smooth profile (cubic polynomial) drawn through the measured liquid temperatures. Liquid side heat flux was then estimated as

$$q_{i-l}(z) - k_l = \frac{\partial T}{\partial y}(z)|_i \tag{3}$$

2.4. Uncertainty estimation

Uncertainty in measured wall heat flux was due to (i) uncertainty in the thermal conductivity of copper, (ii) uncertainty in the temperature gradient in the copper block and (iii) uncertainty due to lack of one-dimensional heat transfer. The uncertainty in the thermal conductivity (k) of the copper block was estimated to be approximately 1%. The maximum uncertainty in the wall heat flux due to lack of one-dimensional heat transfer was estimated from the measured temperature profiles in the solid to be about 7% for all the axial locations except for at the inlet and at the exit of the test section. Close to the inlet and the exit of the test section, the uncertainty due to lack of one-dimensional conduction was about 12%. The uncertainty in temperature gradient inside the copper block is due to (i) uncertainty in temperature measurement and (ii) uncertainty in thermocouple placement. The uncertainty in temperature measurement was estimated to be ±0.2 °C. The uncertainty in the placement of thermocouples in the copper block was estimated to be ±0.5 mm. Based on these uncertainties, the error in the calculated q_w of 7.1, 15 and 20 W/cm^2 are ±15.1%, ±10.7% and ±8.6% and respectively. The maximum uncertainty in the calculated heater surface temperatures estimated to be about ±0.9 °C for the case of G = 700 kg/m^{2}s, ΔT_w = 350 °C and ΔT_{sub} = 24.5 °C. Based on the uncertainties in q_w and T_w, the uncertainty in h_w is estimated to be about 15.2% for h_w = 260 W/m^{2}K which corresponds to the lowest value of h_w measured in the present study. As h_w increases, the uncertainty in h_w decreases and hence 15.2% is the maximum uncertainty in the estimation of h_w. Details of thermocouple calibration and uncertainty calculations can be found in [15].

Liquid side temperature gradient was estimated by calculating the gradient at the vapor–liquid interface of a smooth profile (cubic polynomial) drawn through the measured liquid temperatures. The uncertainty in q_{i-l} is due to (i) uncertainty in thermal conductivity of the liquid and (ii) uncertainty in the estimation of the slope of the profile, $(\partial T/\partial y)$. The uncertainty in the thermal conductivity of the liquid is about 1%. The uncertainty in estimation of $(\partial T/\partial y)_i$ is due to the error in estimation of parameters of the non-linear curve fit. This error was estimated using JMP Statistical Analysis Software. For G = 175 kg/m^{2}s, ΔT_w = 270 °C, ΔT_{sub} = 4.8 °C the error in $(\partial T/\partial y)_i$ was estimated to be about 14.2%. Consequently, the uncertainty in liquid side heat flux (q_{i-l} = 6.3 W/cm^2) was estimated to be 14.4%. For G = 350 kg/m^{2}s, ΔT_w = 270 °C and ΔT_{sub} = 15.2 °C, the estimated error in $(\partial T/\partial y)_i$ was found to be 10.8% thus giving rise to an uncertainty in the measured liquid side heat flux (q_{i-l} = 14.8 W/cm^2) of 10.9%.

3. Results and discussion

3.1. Wall heat flux partitioning during subcooled film boiling

Various heat transfer components during subcooled film boiling are schematically shown in Fig. 2. The heat transfer process in film boiling is a three-step process: heat transfer from wall to vapor ($q_{w\text{-}v}$), from vapor to interface ($q_{v\text{-}i}$) and interface to liquid core (q_{i-l}). In addition to these, heat is transferred directly from the wall to the interface through radiation (q_{rad}). These components are related to each other as follows (from [16]):

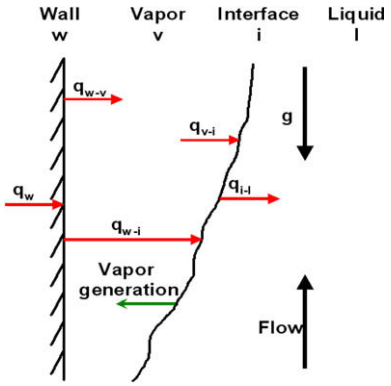

Fig. 2. Heat transfer modes during subcooled film boiling.

$$Q_w = q_w A_w = q_{w-v} A_w + q_{rad} A_w \quad (4)$$

$$Q_{v,conv} = q_{v,conv} A_w = q_{w-v} A_w - q_{v-i} A_i \quad (5)$$

$$Q_{evap} = q_{evap} A_i = q_{v-i} A_i + q_{rad} A_w - q_{i-l} A_i \quad (6)$$

In the range of wall superheats studied in this work, q_{rad} (Appendix A) and $q_{v,conv}$ (Appendix B) are negligible. Also assuming $A_w \approx A_i$, Eqs. (4)–(6) can be simplified to,

$$q_w = q_{i-l} + q_{evap} \quad (7)$$

In the present study, q_w and q_{i-l} were measured independently from the temperature profiles inside the copper block and the liquid temperature profiles, respectively. The evaporative heat flux (q_{evap}) was then estimated by subtracting q_{i-l} from q_w. The experimental results of q_w and q_{i-l} will be discussed in Sections 3.1.1 and 3.1.4, respectively.

3.1.1. Wall heat flux (q_w) and film boiling heat transfer coefficient (h_w)

Flow film boiling experiments with water at atmospheric pressure were conducted under steady state conditions for G varying from 0 to 700 kg/m^{2}s, ΔT_w varying from 0 to 25 °C and ΔT_w varying from 200 to 350 °C. Measurements of q_w and T_w were made at seven different axial locations. In this paper, $\Delta T_{sub,in}$ refers to the inlet liquid subcooling whereas, ΔT_{sub} refers to the local liquid subcooling at any given axial location. For a given inlet subcooling, $\Delta T_{sub,in}$, the local liquid subcooling, ΔT_{sub}, can be estimated at any location downstream as shown in Appendix C.

3.1.2. Effect of axial location (z), massflux (G), liquid subcooling (ΔT_{sub}) and wall superheat (ΔT_w) on heat transfer coefficient

In Fig. 3 measured h_w values are plotted as a function of distance from the leading edge for three values of $\Delta T_{sub,in}$ for constant ΔT_w and G. In this figure, for comparison, h_w predicted from a two-phase laminar boundary layer analysis [2] are also plotted. It is seen that the two-phase laminar boundary layer analysis underpredicts the experimental wall heat transfer results. Also the experimentally obtained h_w varies weakly with distance from the leading edge (z), whereas the two-phase boundary layer analysis suggests that the heat transfer coefficient varies as $z^{-0.25}$.

The experimental results showing weak dependency of h_w on z have been reported for film boiling on a vertical surface by a number of researchers [7,8,10,19]. Bui and Dhir [7] explained the reason for this behavior as follows: Near the leading edge, the interface is free of any waves and two-phase boundary layer type analysis [2,5,17] is applicable for the film. The heat transfer coefficient very close to the leading edge is thus a function of distance from the leading edge but is independent of time. At short distances from the leading edge, waves with both long and short

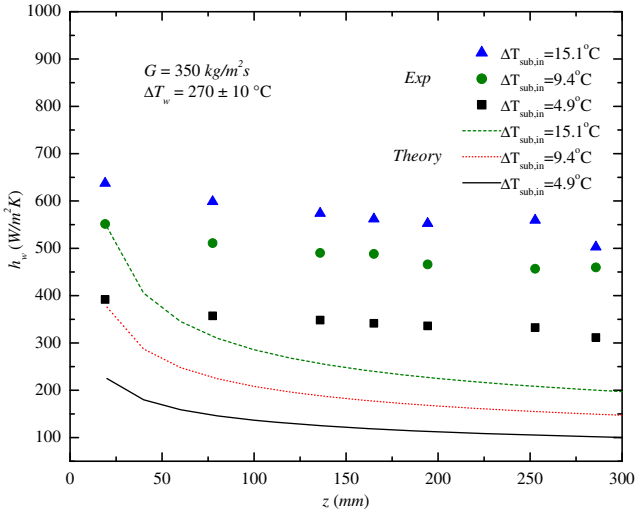

Fig. 3. Experimental wall heat transfer coefficient results – comparison with two-phase boundary layer theory [2].

wavelengths develop. Vapor bulges or bubbles and ripples sweep a given location on the wall alternatively. Since the rates of heat transfer under the bubble and the film are different, the heat transfer coefficient at a given location is time dependent. Hence, a time-averaged h_w value is independent of distance from the leading edge.

Photographs showing the wavy structure of the interface are shown in Fig. 4. This figure shows a front view of the interface for G = 350 kg/m^{2}s, ΔT_w = 250 °C and ΔT_{sub} = 0.8 °C, 4.7 °C and 9.5 °C. For ΔT_{sub} = 0.8 °C, the interface is covered with both large-scale and small-scale waves. As ΔT_{sub} is increased, the amplitude of the large-scale waves shrinks and for the case of ΔT_{sub} = 9.5 °C, the large-scale waves cannot be differentiated from the ripples any more and the entire interface is comprised of two dimensional ripples. Similar interfacial wave pattern was also observed in the study by Bui and Dhir [7] and Vijaykumar and Dhir [8].

From the motion pictures of the vapor–liquid interface, information on distance required for formation of waves was also obtained. It was observed that ΔT_w, ΔT_{sub} and G had an effect on the distance for the formation of the waves (l_{waves}). Increasing ΔT_{sub} and G increased l_{waves}, whereas increasing ΔT_w decreased l_{waves}. Data for l_{waves} for various conditions of ΔT_w, ΔT_{sub} and G were obtained and the following correlation was developed for l^* (non-dimensional distance for formation of the waves).

$$l^* = 2.19(1 + 0.0005\mathrm{Re}_l)(1 - 1.61Ja_{sup})(1 + 313.6Ja_{sub}) \quad (8)$$

Details of this correlation and the data for l_{waves} are given in [15]. This correlation is valid only for water in the following range of conditions: $0 \leqslant Re_l \leqslant 5500$, $0 \leqslant Jas_{ub} \leqslant 0.046$, $0.19 \leqslant Ja_{sup} \leqslant 0.28$. This correlation gives an estimate for the axial location beyond which h_w is independent of z. For $z^* < l^*$, h_w is dependent on z^* whereas for $z^* > l^*$, h_w is independent of z^*. Most data points obtained in the present study belong to the range $z^* > l^*$.

The wall heat transfer coefficient, h_w, was found to be a strong function of ΔT_{sub}, G and ΔT_w. In Fig. 5, the effect of ΔT_{sub}, G and ΔT_w on h_w is plotted. The wall heat transfer coefficient, h_w, increases with increasing ΔT_{sub} and G but decreases with increasing ΔT_w. The data indicates a linear dependence of h_w on ΔT_{sub}. The slope of these lines decreases with increasing ΔT_w, indicating that the effect of ΔT_{sub} decreases with increasing ΔT_w. This is consistent with the observations of [7,8] and is due to increased thickness of the vapor film.

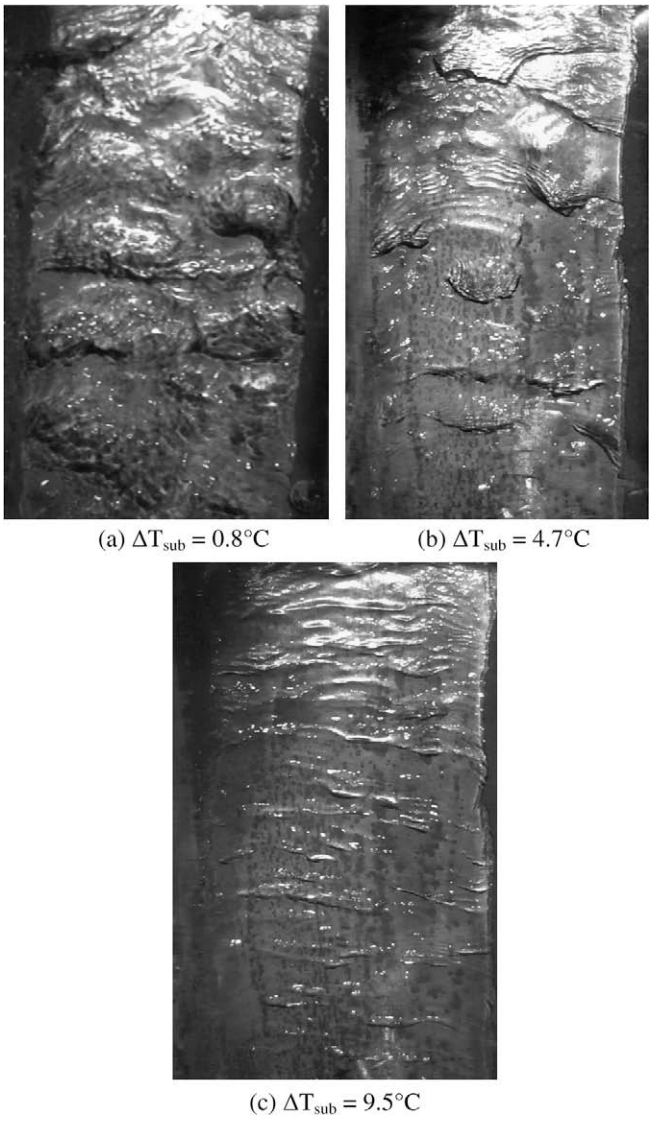

Fig. 4. Visual observations of film boiling. Interfacial waves for $G = 350$ kg/m^{2}s, $\Delta T_w = 250$ °C, $z = 100$ mm and (a) $\Delta T_{sub} = 0.8$ °C, (b) $\Delta T_{sub} = 4.7$ °C and (c) $\Delta T_{sub} = 9.5$ °C.

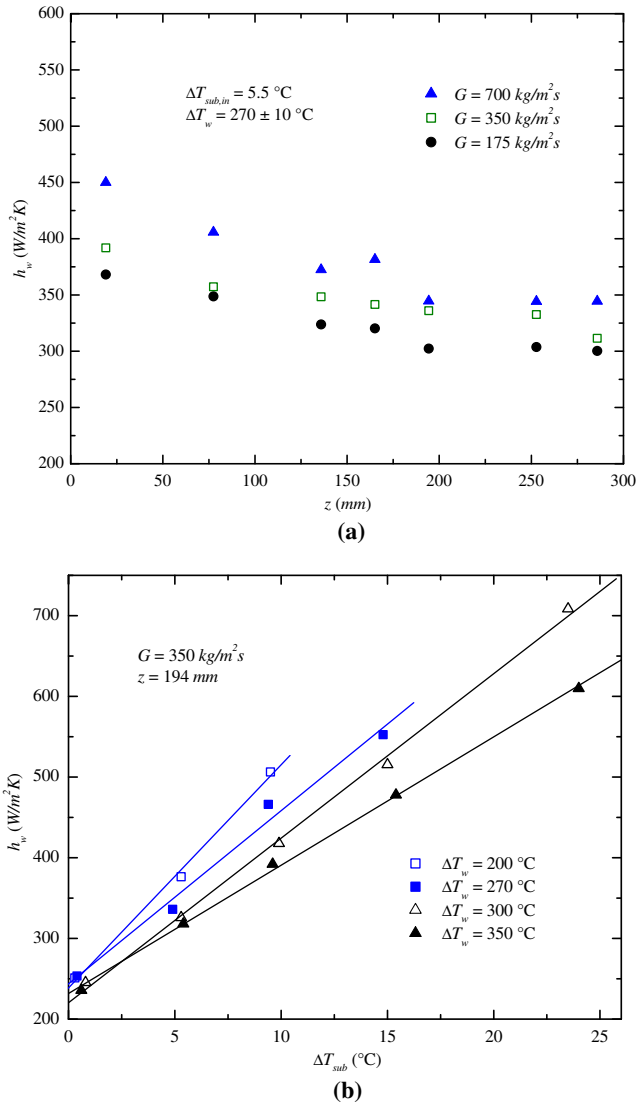

Fig. 5. (a) Effect of mass flux and (b) effect of wall superheat and liquid subcooling on wall heat transfer coefficient.

3.1.3. Correlation for wall Nusselt Number (Nu_w) and comparison with data

The wall heat transfer coefficient data for $z^* > l^*$ was first non-dimensionalized to obtain Nu_w and 180 data points were correlated by the following expression:

$$Nu_w = 0.4\left(\frac{L_c^3 g(\rho_l-\rho_v)^2 C_{pv}}{k_v \mu_v}\right)^{-1/4} Ja_{sup}^{-1/4}\left(1+7\frac{Ja_{sub}}{Ja_{sup}^{1.5}}\right)\left(1+0.0055Re_l^{0.5}\right) \quad (9)$$

The form of the above correlation was chosen by taking into consideration the asymptotic limits of $\Delta T_{sub} = 0$ °C and $Re_l = 0$. When both $\Delta T_{sub} = 0$ °C and $Re_l = 0$, Nu_w from Eq. (9) predicts film boiling heat transfer for saturated pool film boiling conditions. When $Re_l = 0$ and $\Delta T_{sub} > 0$ °C, Eq. (9) predicts the film boiling Nu_w for subcooled pool film boiling. As will be shown later, predictions from Eq. (9) compare very well with the data from experiments for both saturated and subcooled pool film boiling conditions. In developing Eq. (9), the linear dependence of Nu_w on ΔT_{sub} and the observation that the slope of this linear function decreases with increasing ΔT_w was taken into account by introducing the term $\left(1+7\frac{Ja_{sub}}{Ja_{sup}^{1.5}}\right)$. This is consistent with the correlation given by Dhir and Purohit [5] for flow film boiling on spheres. The dependence of Nu_w on $Re_l^{0.5}$ is also consistent with [5,18].

This correlation was developed primarily for water at atmospheric pressure and is valid in the following range of conditions: $z^* > l^*$, $0 \leqslant Re_l \leqslant 5500$, $0 \leqslant Ja_{sub}$ 0.046, $0.19 \leqslant Ja_{sup} \leqslant 0.28$. Comparison of Nu_w predicted using Eq. (9) with experimental data from the present work is shown in Fig. 6. Using Eq. (9), the present experimental data can be predicted to within ±20%.

An attempt was also made to extend this correlation to other fluids by adopting the method proposed by Bui and Dhir [7] and hence introducing the factor $\left(\frac{L_c^3 g(\rho_l-\rho_v)^2 C_{pv}}{k_v \mu_v}\right)$. Fig. 7 shows comparison of Eq. (9) with the Freon-113 data of Aritomi et al. [14]. In their experiments, the effect of U_l and ΔT_{sub} on the axial variation of h_w was studied. Even though Eq. (9) is developed for Nu_w that is independent of z, Fig. 7 indicates that both the experimental h_w and the predicted h_w show a strong dependence on z. This is due to the axial variation of ΔT_w in their experiments. This figure shows that the effects of U_l and ΔT_{sub} are captured well by Eq. (9), even for Freon-113.

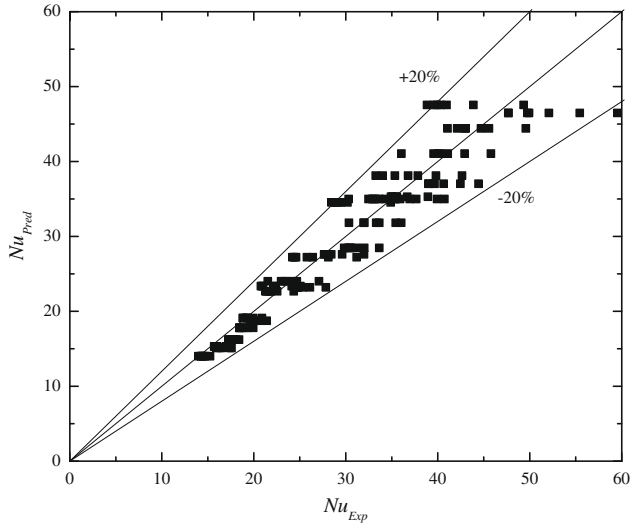

Fig. 6. Correlation of wall heat transfer coefficient data – comparison of predictions with experimental data of the present work obtained with water as the test liquid.

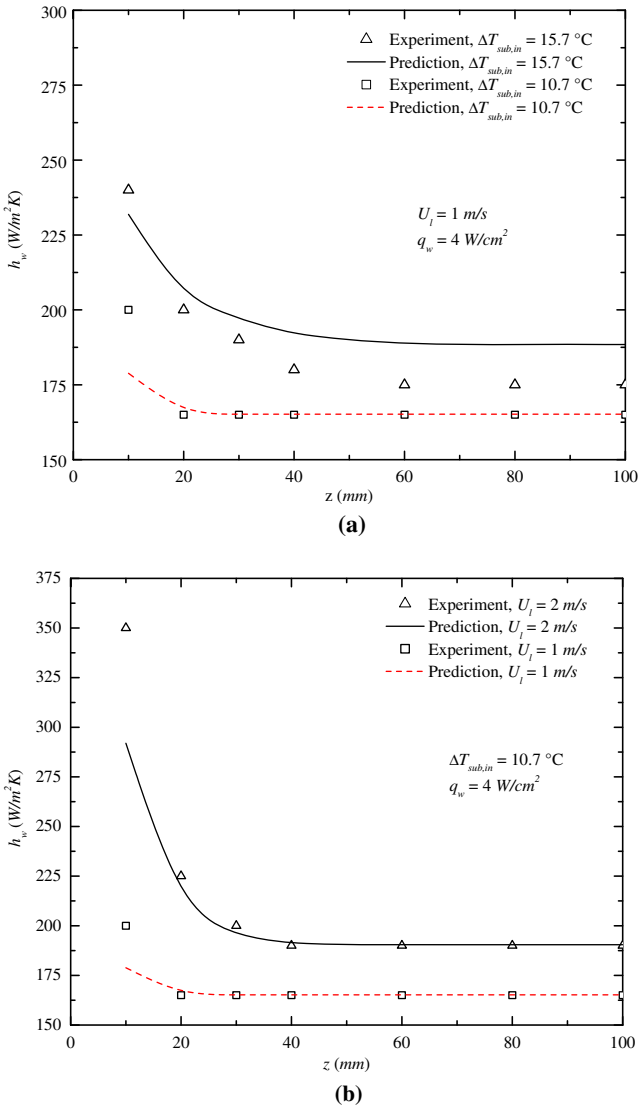

Fig. 7. Comparison of predictions from Eq. (9) with Freon-113 data of Aritomi et al. [14] (a) Effect of ΔT_{sub} on h_w and (b) Effect of U_l on h_w.

In Fig. 8, Eq. (9) is compared with various other data sets that involve film boiling at higher system pressures [10], and Freon-113 data [19,14]. The experimental conditions and range of parameters studied in these experiments are given in Table 1. Fig. 8 shows that Eq. (9) agrees well with the experimental data and predicts the data to within ±25%. Detailed calculations that show the comparison of the predictions from Eq. (9) with the experimental data from the present work and from the literature can be found in [15].

3.1.4. Liquid side heat transfer and evaporation heat flux

The fluid temperature profiles were measured at five different axial locations using traversable microthermocouples. The typical response time of these thermocouples is about 5–7 ms. Fig. 9 shows the vapor and liquid temperature profiles at an axial location of 64.8 mm from the leading edge. The traversable microthermocouples were first moved in towards the heater surface till they just touch the surface and then they were moved out in steps of 0.025 mm till they measure the bulk liquid temperature. At every position of the thermocouple, the temperatures were recorded for 30 s. At any given position, the maximum variation in the fluid temperatures was ±1.5 °C [15]. In Fig. 9(a), time averaged T_{fluid} data (over a period of 30 s) are plotted as a function of distance from the heater surface (y). Fig. 9(b) is a zoomed view of Fig. 9(a) highlighting the part of the fluid temperature profile close to the vapor–liquid interface and inside the liquid boundary layer. From Fig. 9(a) it is clear that a large temperature gradient exists close to the heated wall. Far from the interface, the fluid temperature is the bulk liquid temperature.

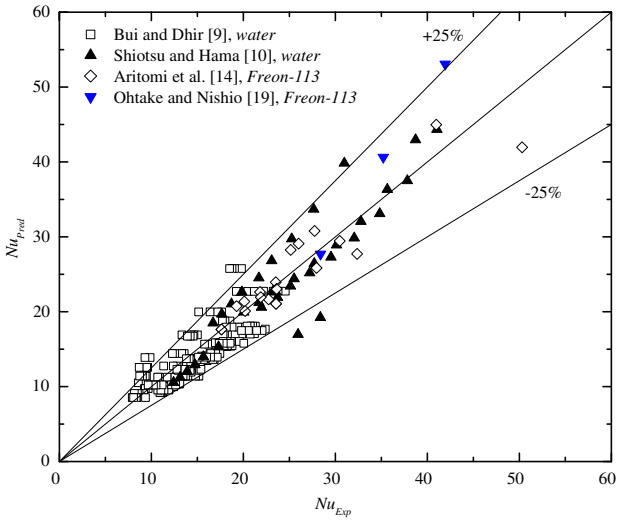

Fig. 8. Comparison of the predicted Nusselt number from Eq. (9) with data from the literature.

Table 1
Experimental conditions for h_w data.

Investigators	Working fluid	P (bar)	G (kg/m^{2}s)	ΔT_{sub} (°C)	T_w (°C)
Present work	Water	1.03	0–700	0–25	250–450
Bui and Dhir [7]	Water	1.03	0	0–25	250–500
Vijaykumar and Dhir [8]	Water	1.03	0	0–25	250–500
Aritomi et al. [14]	R-113	1.03	778–3112	10.7–20.7	150–300
Ohtake and Nishio [19]	R-113	1.03	0	0–30	107–207
Shiotsu and Hama [10]	Water and R-113	1.02–4.9	0–4668	0–60	250–450

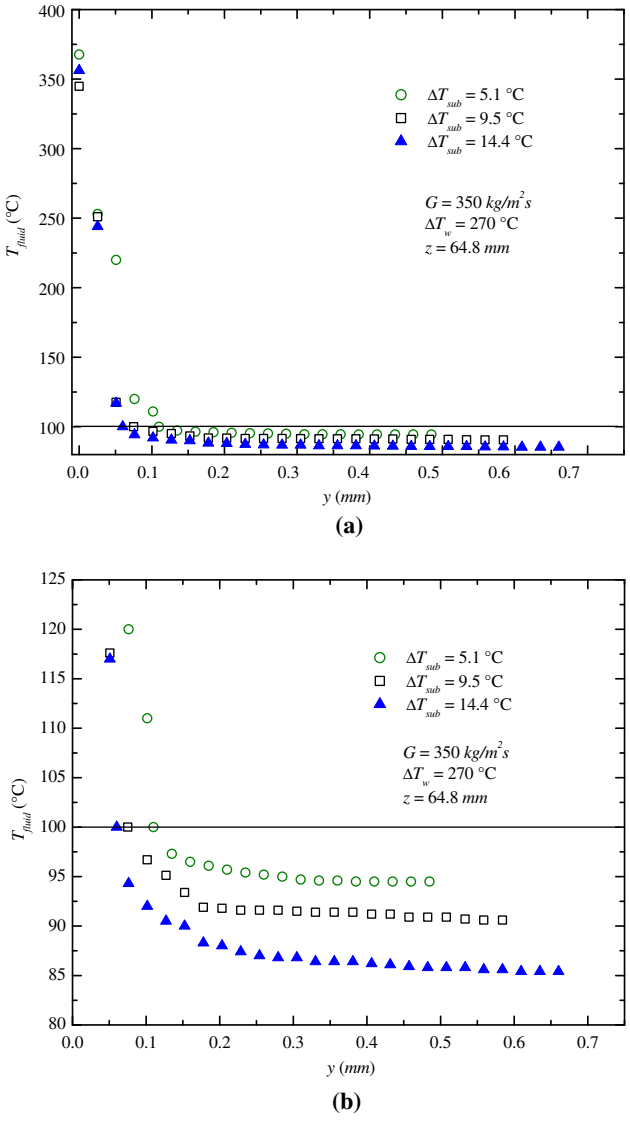

Fig. 9. Time averaged fluid temperature profiles for three different liquid subcoolings: (a) expanded view, (b) zoomed view.

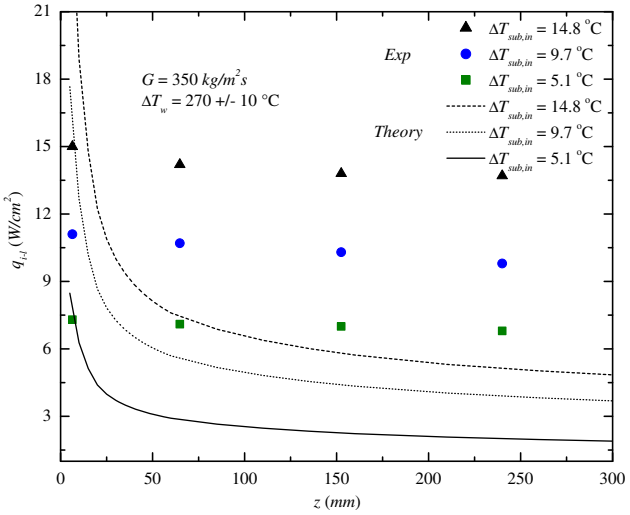

Fig. 10. Liquid side heat transfer – Effect of z and comparison with two-phase boundary layer theory (2).

Wall heat flux (q_w) and liquid side heat flux (q_{i-l}) were estimated from the fluid temperature profiles. Wall heat flux (q_w) was estimated by calculating the temperature gradient in the vapor film. Wall heat flux (q_w) thus calculated was found to be within ±15% of the wall heat flux estimated using the thermocouples embedded in the copper block. Liquid side temperature gradient was estimated by calculating the gradient at the vapor–liquid interface of a smooth profile (cubic polynomial) drawn through the measured liquid temperatures. Liquid side heat flux was then estimated using Eq. (3). For the temperature profiles shown in Fig. 9(b), the liquid side temperature gradients were estimated to be 106.1, 165.1, 227.3 °C/mm and the corresponding q_{i-l} were estimated to be 7 W/cm^2, 10.9 W/cm^2 and 14.6 W/cm^2 for ΔT_{sub} = 5.1, 9.7 and 14.8 °C, respectively.

Fig. 10 shows a comparison of the measured liquid side heat flux at three different ΔT_{sub} values with that obtained from two-phase boundary layer theory [2]. Measured q_{i-l} values show a much weaker dependence on axial location when compared to that predicted from theory. It must be mentioned here that the liquid side heat transfer estimated in the present study is only a time-averaged value. In reality, the presence of interfacial waves would make the liquid side heat transfer transient. Vijaykumar and Dhir [8], using holographic interferometry, obtained measurements of liquid side heat transfer. They observed that the liquid side heat transfer is maximum at the peaks of the wavy interface and minimum at the wave valleys. They explained that most of the evaporation occurs in the valleys and some of the vapor produced in the valleys is condensed at the peaks.

The effect of ΔT_{sub}, G and ΔT_w on q_{i-l} and q_{evap} is illustrated in Fig. 11. Measured q_{i-l} values were found to be a strong function of ΔT_{sub} and G, but a weak function of ΔT_w. In the present study, no systematic effect of ΔT_w on q_{i-l} was observed. This could be explained by carrying out an energy balance on the vapor–liquid interface. Following Dhir and Purohit [5], the liquid side heat flux can be expressed as,

$$q_{i-1} = -k_l \left.\frac{\partial T - l}{\partial y}\right|_{y=\delta} = \frac{d}{dz}\int_0^{\delta_l} U_l \rho_l C_{pl} \Delta T_{sub} dy \qquad (10)$$

From Eq. (10), it can be seen that increasing U_l or ΔT_{sub} would result in an increase in the integrand and hence q_{i-l} would increase. Increase in wall superheat tends to increase the interfacial velocity and hence the average velocity in the liquid boundary layer. This would then increase q_{i-l}. However, in the range of wall superheats studied in this work, interfacial velocity, as measured from the motion pictures of the vapor–liquid interface, increases only slightly. For example, for G = 350 kg/m^{2}s and ΔT_{sub} = 5 °C the interfacial velocity at ΔT_w = 210 °C was 0.9 m/s whereas at ΔT_w = 320 °C the interfacial velocity was 1.1 m/s [15]. Consequently, the measured q_{i-l} was found to be very weakly dependent on ΔT_w.

In Fig. 11, variation of q_{evap} with ΔT_{sub}, G and ΔT_w is also plotted. For the range of ΔT_w studied in the present work, since $q_{v,conv}$ was estimated to be within the uncertainty level of q_w (Appendix B), it is assumed that the total wall heat flux (q_w) is divided between heat flux into the liquid (q_{i-l}) and heat flux into vapor generation (q_{evap}). Hence, $q_w = q_{i-l} + q_{evap}$. Since q_w and q_{i-l} were measured independently, q_{evap} can be obtained as,

$$q_{evap} = q_w - q_{i-l} \qquad (11)$$

It was found that for fixed ΔT_w, q_{evap} decreases as ΔT_{sub} or G increases. This is reflected in the measured film thickness, δ which decreases when either ΔT_{sub} or G is increased.

Complete details of all the experimental data obtained in the present work can be found in [15]. Based on the present data, a correlation for q_{i-l}/q_w was developed as a function of Ja_{sub}, Re_l and Ja_{sup}. This correlation is given as,

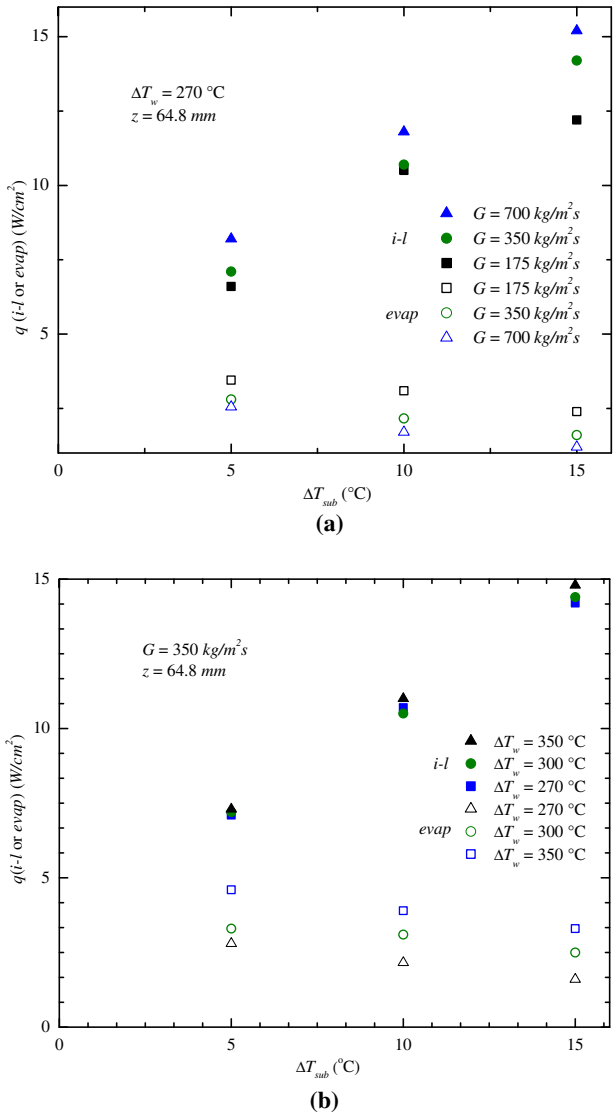

Fig. 11. Effect of (a) G and ΔT_{sub} and (b) ΔT_w and ΔT_{sub} on q_{i-l} and q_{evap}.

$$\frac{q_{i-l}}{q_w} = 0.012\left(\frac{\rho_l}{\rho_v}\right)^{0.5} Pr_l^{0.2}\frac{Ja_{sub}^{0.2}Ja_{sup}^{-0.6}(1+0.0005Re_l^{0.75})}{(1+7.7\exp(-512Ja_{sub}))} \quad (12)$$

The form of Eq. (12) was chosen by considering the following asymptotic limits: As $Ja \to 0$, $q_{i-l}/q_w \to 0$, and as $Re_l \to 0$, predictions from Eq. (12) should correspond to q_{i-l}/q_w values for subcooled pool film boiling [8]. The factors $(\rho_l/\rho_v)^{0.5}$ and $Pr_l^{0.2}$ were introduced to account for the effects of pressure and fluid properties on wall heat flux partitioning.

In Fig. 12, Eq. (12) is compared with the present experimental data and with the data of [8]. It can be seen that both these data sets are predicted within ±20%. Further comparison of the correlation with experimental data was not possible due to lack of experimental data on liquid side heat transfer. To the best of our knowledge, the only experimental data available so far on liquid side heat transfer are the present data and the data of [8].

In order to further validate Eq. (12), a correlation for wall superheat at film collapse (ΔT_{fc}) was deduced from Eq. (12). The motivation behind the correlation for ΔT_{fc} is as follows: For fixed ΔT_w and G, increasing ΔT_{sub} results in more heat going into the liquid. Hence, q_{evap} decreases. At sufficiently high ΔT_{sub}, say at $\Delta T_{sub,fc}$, the vapor generation rate would become so small or negative that

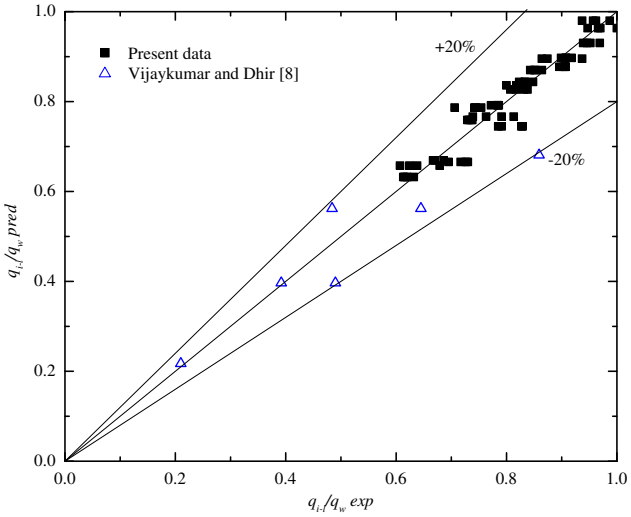

Fig. 12. Correlation of liquid side heat transfer – Comparison of the predicted q_{i-l}/q_w with experimental values of q_{i-l}/q_w.

stable film boiling cannot be sustained and hence the vapor film collapses. In other words, for given G and $\Delta T_{sub} = \Delta T_{sub,fc}$, the corresponding ΔT_w would give an estimate for $(\Delta T_w)_{fc}$.

To illustrate the film collapse conditions, the ratios q_{i-l}/q_w and q_{evap}/q_w obtained from experimental data as well as those predicted from Eq. (12) are plotted in Fig. 13, as a function of ΔT_{sub} for various ΔT_w values. For fixed ΔT_w, the film collapse occurs at ΔT_{sub} for which $q_{i-l}/q_w = 100\%$. For example, for $\Delta T_w = 270$ °C and $G = 350$ kg/m^{2}s, ΔT_{sub} at film collapse was estimated to be about 22 °C. From the experiments, it was observed that for $\Delta T_w = 270$ °C and $G = 350$ kg/m^{2}s, it was not possible to achieve stable film boiling for $\Delta T_{sub} > 20$ °C.

3.2. Correlation for minimum film collapse temperature, $(T_w)_{fc}$

In this section, a correlation deduced from Eq. (12) will be presented and will be validated against the data and models available in the literature. By equating q_{i-l}/q_w to 1 in Eq. (12), and rearranging the terms we get,

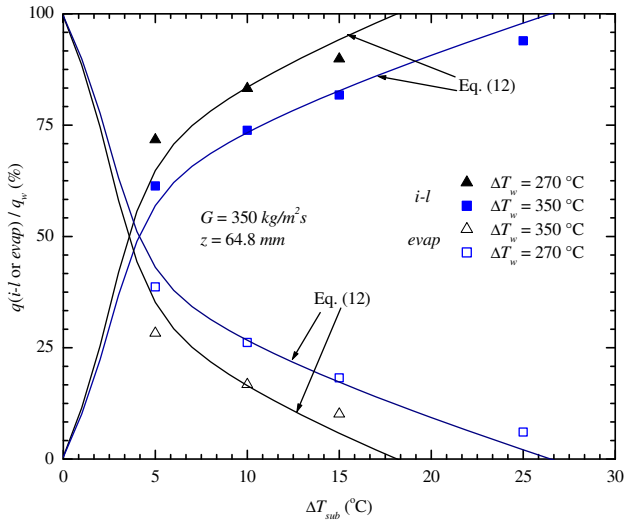

Fig. 13. Effect of ΔT_{sub} and ΔT_w on wall heat flux partitioning and deduction of minimum film collapse temperature from wall heat flux partitioning data.

$$(Ja_{sup})_{fc} = 0.0006\left(\frac{\rho_l}{\rho_v}\right)^{0.83} Pr_l^{0.33} \frac{ja_{sub}^{0.33}(1+.0005Re_l^{0.75})^{1.67}}{(1+7.07\exp(-512ja_{sub}))^{1.67}} \quad (13)$$

The minimum wall superheat at film collapse is then given by,

$$(\Delta T_w)_{fc} = \frac{h_{fg}}{Cp_v}\left(0.0006\left(\frac{\rho_l}{\rho_v}\right)^{0.83} Pr_l^{0.33} \frac{Ja_{sub}^{0.33}(1+.0005Re_l^{0.75})^{1.67}}{(1+7.7\exp(-512Ja_{sub}))^{1.67}}\right) \quad (14)$$

It must be noted that Eq. (14) is only valid for subcooled conditions. This is because, as $\Delta T_{sub} \to 0$ (saturated conditions), $q_{i-l}/q_w \to 0$ and hence the basic premise of the model ($q_{i-l}/q_w = 1$) will never be satisfied. To extend the present correlation to saturated and low subcooling cases, an expression for $(\Delta T_w)_{fc}$ given by Carbajo [20] for saturated conditions is added to Eq. (14) resulting in the following form for $(\Delta T_w)_{fc}$,

$$(\Delta T_w)_{fc} = (\Delta T_{w,sat})_{fc} + \frac{h_{fg}}{Cp_v}\left(0.0006\left(\frac{\rho_l}{\rho_v}\right)^{0.83} \times Pr_l^{0.33} \frac{Ja_{sub}^{0.33}(1+.0005Re_l^{0.75})^{1.67}}{(1+7.7\exp(-512Ja_{sub}))^{1.67}}\right) \quad (15)$$

where

$$(\Delta T_{w,sat})_{fc} = \frac{1.372\times 10^6}{T_{cr}^{2.3}}\left(\frac{T_{cr}-T_{sat}}{\sqrt{\mu_l}}\right)^{0.5}(1+0.043Re_l^{0.4}) \quad (16)$$

Fig. 14 shows a comparison of the proposed model for $(T_w)_{fc}$ with previous correlations available in the literature. The correlations of Drucker and Dhir [21] and Dhir and Purohit [5] were developed for water at atmospheric pressure for rod bundle and spherical geometries respectively. Cheng et al.'s [22] correlation was developed for water flowing in a vertical tube, but is valid for a wide range of pressures. The results from current approach compare well with the correlations given in [21] and [5] and are generally higher than the predictions given in [22]. The deviation with Cheng et al.'s correlation could be because their correlation was developed using experimental data obtained at pressures higher than one atmospheric pressure while the comparison in Fig. 14 is made for a pressure of one atmosphere. The present correlation also yields a non-linear increase in $(T_w)_{fc}$ with ΔT_{sub} for low ΔT_{sub} ($\Delta T_{sub} < 5$ °C) and a linear increase in $(T_w)_{fc}$ with ΔT_{sub} for high ΔT_{sub} ($\Delta T_{sub} > 5$ °C). Interestingly, a similar effect of ΔT_{sub} is predicted by the theoretical model given in [23].

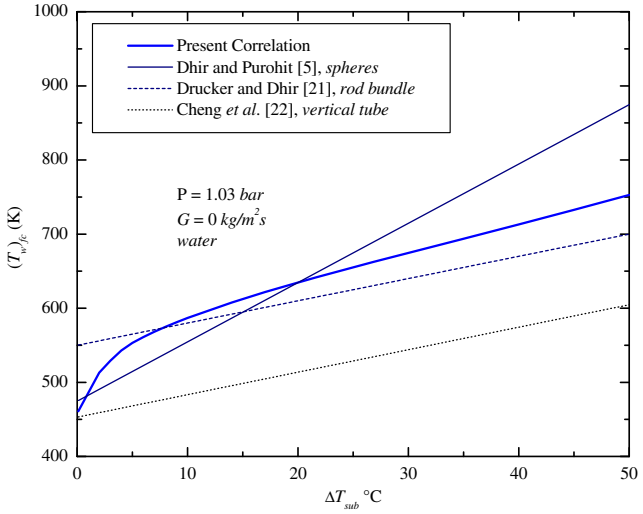

Fig. 14. Comparison of predicted $(T_w)_{fc}$ values with correlations available in the literature.

Fig. 15 shows a comparison of predicted and measured $(T_w)_{fc}$. The data from [22] were obtained using water at a pressure of 3.44 bar. It can be seen that the proposed model describes the effect of mass flux on $(T_w)_{fc}$ correctly even at pressures that are different from one atmosphere. The data from (Fig. 16), the predicted $(T_w)_{fc}$ for Freon-113 is compared with the Freon-113 data of [24]. Once again, the predictions from Eq. (15) are in good agreement with data from experiments except at low mass velocities.

3.3. Effect of system pressure

Fig. 16 shows the effect of pressure on predicted partitioning of wall heat flux (Fig. 16 (a)) and total wall heat flux (Fig. 16 (b)). In Fig. 16 (b), for the cases of $P = 1$ bar and $P = 2$ bar, the plots of q_w versus ΔT_{sub} do not extend beyond $\Delta T_{sub} = 22$ °C and $\Delta T_{sub} = 53$ °C, respectively. This is because for $P = 1$ bar and P = 2 bar, q_{i-l}/q_w=1 at $\Delta T_{sub} = 22$ °C and 52 °C respectively indicating that stable film boiling is not possible for higher ΔT_{sub} for the given ΔT_w and G. Fig. 16 shows that for fixed ΔT_w and G, q_w increases as pressure increases, whereas q_{i-l}/q_w decreases as pressure increases. In general, as pressure increases, the fluid property group, $\rho_v h_{fg}$, increases

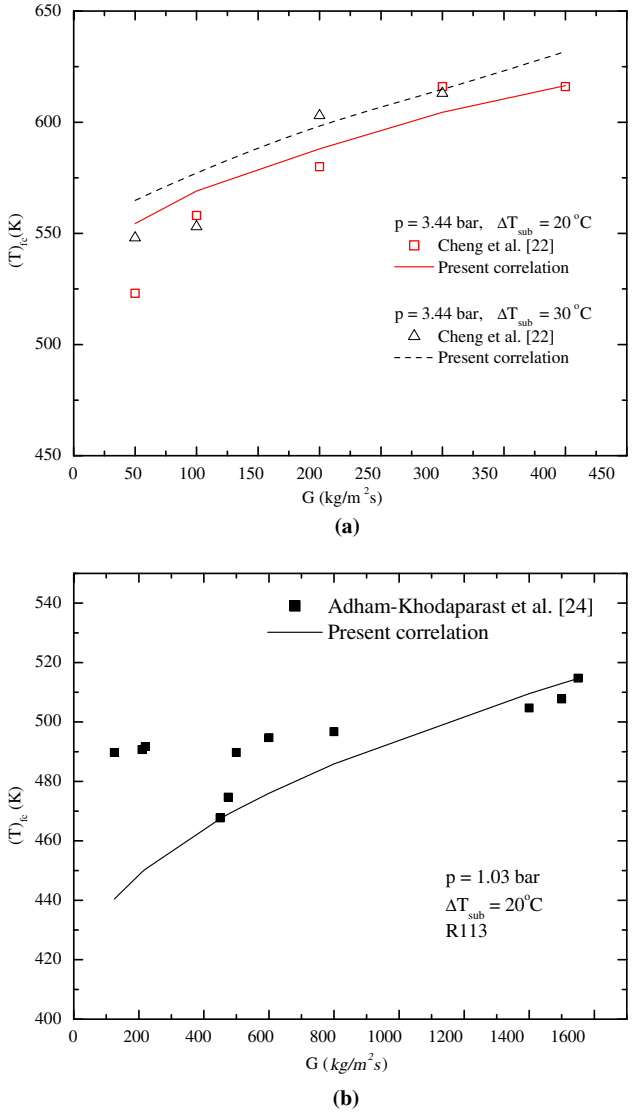

Fig. 15. Comparison of $(T_w)_{fc}$ values predicted from Eq. (15) with experimental data in the literature: (a) data from [22] (fluid: water) and (b) data from [24] (fluid: R113).

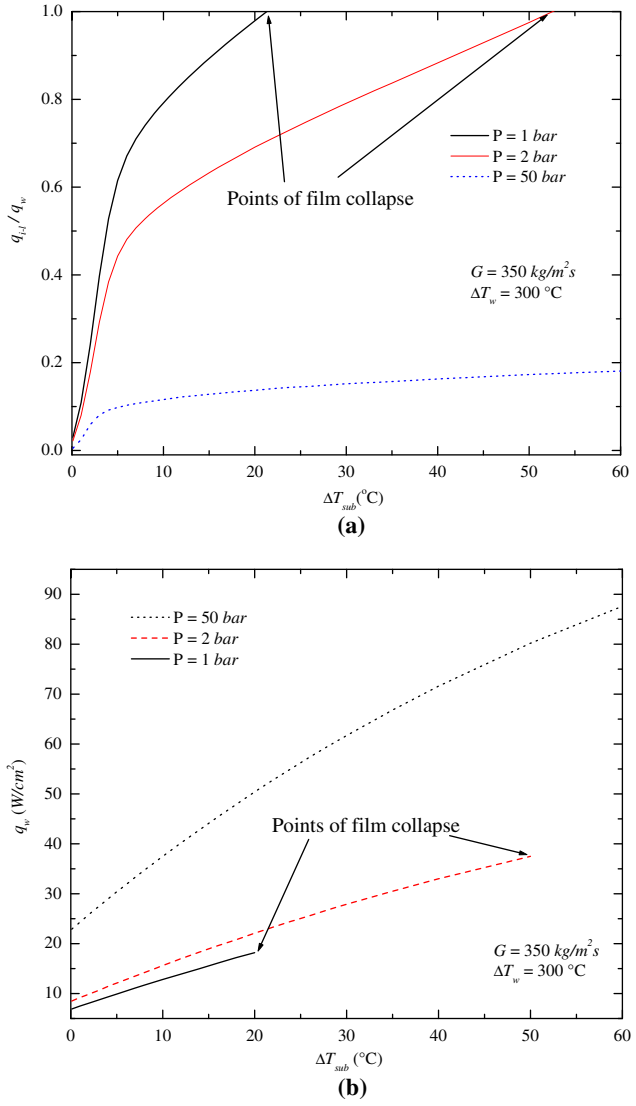

Fig. 16. Effect of pressure and liquid subcooling on (a) wall heat flux partitioning, and (b) wall heat flux.

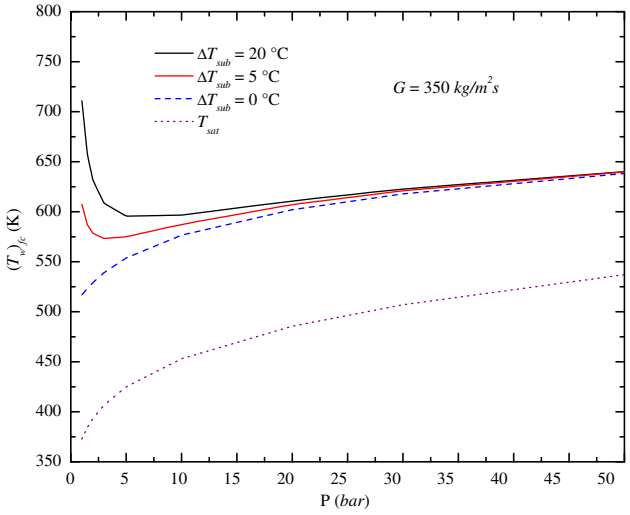

Fig. 17. Effect of pressure and liquid subcooling on $(T_w)_{fc}$.

significantly (for example, for water, as pressure increases from 1 bar to 100 bars, $\rho_v h_{fg}$ increases by about 50 times). This in turn increases the heat flux carried away by the vapor due to convection thus reducing the fraction of heat taken away by the liquid. Even though the contribution of q_{conv} to q_w was ignored for the range of experimental conditions studied in the present work, it is still possible to comment on the role played by q_{conv} while explaining the effect of system pressure on q_{i-l}/q_w. This is because, the assumption of $q_{conv} \simeq 0$ was made only while estimating q_{evap} from q_w and q_{i-l}. Such an assumption was not made while developing the correlations for q_w and q_{i-l}/q_w. From Fig. 16, it can also be seen that at higher pressures, the effect of ΔT_{sub} on $q_{i-l}/q_w \to 0$ decreases. This is due to the fact that ΔT_{sub} tends to increase the rate of liquid side heat transfer but as system pressure increases, the percentage contribution of q_{i-l} to q_w decreases and in turn we see a smaller effect of ΔT_{sub} at higher pressures.

In Fig. 17, the effect of varying the pressure on the model prediction of $(T_w)_{fc}$ is shown. As the pressure increases, $(T_w)_{fc}$ first decreases and then starts increasing. This pattern is more apparent for higher ΔT_{sub}. As ΔT_{sub} decreases, the initial decrease in $(T_w)_{fc}$ with pressure becomes less apparent and for $\Delta T_{sub} = 0$ °C, $(T_w)_{fc}$ increases monotonically with pressure. This increase is consistent with Sakurai et al. [25]. From this figure, it can also be seen that, as pressure increases, the effect of ΔT_{sub} on $(T_w)_{fc}$ decreases and it is found that for $P > 30$ bar, there is little effect of ΔT_{sub} on $(T_w)_{fc}$. This behavior is consistent with the predictions of Carbajo [20].

It should be noted that the effects of surface roughness and oxidation level on $\Delta(T_w)_{fc}$ are not incorporated in Eq. (15). Sinha et al. [26] conducted quenching experiments on Inconel-Al_2O_3 and Zircaloy-BN fuel rods and studied the effects of liquid subcooling, surface roughness and surface oxidation on the minimum film boiling temperature. In general, it was observed that increasing levels of roughness or surface oxidation tend to result in higher values of $(T_w)_{fc}$. They explained that close to the minimum film boiling point, the vapor film thickness decreased, and it was possible for the wall roughness elements to interact with the liquid–vapor interface. The roughness elements might have tripped the liquid–vapor interface, enhancing surface-liquid contact. From their work, it is quite evident that surface roughness and a thicker oxide layer allowed quenching to occur at a considerably higher temperature. Since Eq. (15) doesn't take into account the surface roughness and oxidation levels, predictions from Eq. (15) give a lower estimate for $\Delta(T_w)_{fc}$ on a real surface that has some degree of roughness and oxidation.

Nevertheless, the validation of the model using experimental data from literature shows good agreement between the predicted and the measured values. The correlation although primarily developed for water at atmospheric pressure, predicts well high pressure data and data for Freon-113. The correlation is also in reasonable agreement with the experimental data for water developed using various heater surface geometries (spheres, rod bundles and vertical tubes). In addition, the subcooling and the mass flux effects given by the model agree well with the trends shown by the experimental data. Future work should be directed towards collecting more experimental data on wall heat flux partitioning using different test fluids and extending the model to those fluids as well.

4. Conclusions

Flow film boiling experiments of water at atmospheric pressure were conducted under steady state conditions for the following range of parameters: $0 \leqslant G \leqslant 700$ kg/m^{2}s, $0 \leqslant \Delta T_{sub} \leqslant 25$ °C and $200 \leqslant \Delta T_w \leqslant 350$ °C. Simultaneous measurements of the wall heat flux, fluid temperature profiles, liquid side heat flux and interfacial wave behaviour were obtained during steady state flow film

boiling on a vertical plate. Based on the results of this study, the following conclusions can be made.

- Film boiling wall heat transfer coefficient strongly depends on mass velocity, liquid subcooling and wall superheat, but is a weak function of axial distance. Heat transfer coefficient varies linearly with liquid subcooling for a given wall superheat. The enhancement in heat transfer, however, is less sensitive to liquid subcooling at higher wall superheats.
- Liquid side heat flux is observed to be strongly dependent on liquid subcooling and mass flux, but was a weak function of axial distance and wall superheat.
- Empirical correlations have been developed for wall heat transfer coefficient and wall heat flux partitioning. These correlations show good agreement with the present experimental data and also with the experimental data available in the literature.
- Additional validation for the correlation for wall heat flux partitioning has been obtained by deriving a new correlation for the minimum film collapse temperature ($(T_w)_{fc}$). Comparison of the proposed correlation with the data and correlations available in the literature show good agreement.

Acknowledgement

This work received support from United States Nuclear Regulatory Commission (USNRC).

Appendix A

A.1. Estimation of heat flux due to radiation from the wall to the vapor liquid interface

The radiation heat flux was estimated as [18],

$$q_{rad} = \frac{\sigma(T_w^4 - T_{sat}^4)}{1/\varepsilon_w + 1/\varepsilon_l - 1} \tag{A.1}$$

Using $\varepsilon_w = 0.05$ [9] and $\varepsilon_l = 0.95$ [18], q_{rad} for $\Delta T_w = 300$ °C, 400 °C are 0.05 W/cm^2 and 0.1 W/cm^2 respectively. This results in the percentage contribution of radiation to the wall heat flux to be less than 2%.

Since there is usually a considerable amount of variation in ε_w of the surface, ε_w was varied from 0.05 to its maximum value of 1.0, to estimate the range of the contribution of q_{rad} to q_w. For the case of $G = 175$ kg/m^{2}s, $\Delta T_{sub} = 0.8$ °C and $\Delta T_w = 350$ °C (maximum ΔT_w studied in this work), for $0.05 < \varepsilon_w < 1.0$, $q_{i-l}/q_w \to 0$ varied from a minimum of 0.8% to a maximum of 16% (for $\varepsilon_w = 1.0$). For higher ΔT_{sub}, since the wall heat flux is higher, the percentage contribution due to radiation is expected to be even lower.

Appendix B

B.1. Energy required for sensible heating of vapor

Heat flux required for sensible heating of vapor was estimated using the following equation,

$$q_{conv,v} = \frac{d}{dz}\int_0^{\delta} \rho_v U_v C_{p_v} \Delta T_v dy \tag{B.1}$$

To obtain an estimate for $q_{conv,v}$, we need expressions for vapor velocity and vapor temperature. An expression for vapor velocity is obtained by solving the y-momentum equation in the vapor boundary layer. After neglecting the inertia terms, the y-momentum equation in the vapor boundary layer can be written as,

$$\frac{\partial^2 U_v}{\partial y^2} = -(\rho_l - \rho_v)g \tag{B.2}$$

Integrating twice using the following boundary conditions: U_v(i=0)=0, and U_v($y=\delta$)=U_i gives,

$$U_v = -\frac{1}{2\mu_v}(\rho_l - \rho_v)g\delta^2\left(\frac{y}{\delta}\right)^2 + \left(U_i + \frac{(\rho_l - \rho_v)}{2\mu_v}g\delta^2\right)\frac{y}{\delta} \tag{B.3}$$

Assuming a linear temperature profile in the vapor film,

$$\Delta T_v = \Delta T_w\left(1 - \frac{y}{\delta}\right) \tag{B.4}$$

substituting Eqs. (B.4) and (B.5) in Eq. (B.1), and evaluating the integral, we obtain,

$$q_{conv,v} = \rho_v C_{p_v} \Delta T_w \left[\frac{U_i}{6} + \frac{(\rho_l - \rho_v)}{8\mu_v}g\delta^2\right]\frac{d\delta}{dz} \tag{B.5}$$

For $G = 175$ kg/m^{2}s, $\Delta T_{sub} = 4.8$ °C, $\Delta T_w = 350$ °C and $z = 6.4$ mm, from the fluid temperature profiles, $\delta = 0.10$ mm and from the motion pictures of the interface, $U_i = 0.8$ m/s. Since at the leading edge ($z = 0$), $\delta = 0$ *mm* and at $z = 6.4$ mm, $\delta = 0.1$ mm [15], an estimate for $d\delta/dz$ can be obtained as $d\delta/dz = 0.1/6.45 = 0.016$. Evaluating the vapor properties at the mean film temperature (= (T_w + T_{sat})/2 = 275 °C) and substituting in Eq. (B.6), we get, $q_{conv,v}$= 0.33 W/cm^2. For this case $q_w = 8.6$ W/cm^2 and hence $q_{conv,v}/q_w$=3.8% which is within the uncertainty level of q_w.

Appendix C

C.1. Estimating Local liquid subcooling

The heat transferred into the liquid is utilized in heating up of the liquid. Hence, at any axial location, z,

$$\dot{m}C_{pl}dT_l = q_{i-l}wdz \tag{C.1}$$

Hence,

$$T_{l,z} - T_{l,inlet} = \Delta T_{sub,inlet} - \Delta T_{sub,z} = \int_1^2 \frac{q_{i-l}w}{\dot{m}C_{pl}}dz \tag{C.2}$$

The local subcooling can now be expressed as

$$\Delta T_{sub,z} = \Delta T_{sub,inlet} - \frac{k_v \Delta T_w w}{L_c \dot{m} C_{pl}}\int_1^2 \left(\frac{q_{i-l}}{q_w}\right)(Nu_w)dz \tag{C.3}$$

In order to estimate local liquid subcooling from Eq. (C.3), expressions for Nu_w and q_{i-l}/q_w were required. However, the change in liquid subcooling needs to be accounted for inorder to develop correlations for Nu_w and q_{i-l}/q_w. Hence, a trial and error process was adopted and the local liquid subcooling at any given axial location was estimated.

In general, the change in liquid subcooling with axial location is higher for higher inlet liquid subcooling for fixed massflux and ΔT_w. For example, for $G = 350$ kg/m^{2}s, $\Delta T_w = 270$ °C, the change in liquid cooling along the entire length of the test section (30 cm) was 0.4 °C, 0.7 °C and 0.9 °C for $\Delta T_{sub,in} = 5.1$ °C, 10.7 °C and 24.5 °C respectively. For the present experimental conditions, the maximum change in liquid subcooling along the length of the test section (30.5 cm) was about 2.3 °C for the case of $G = 175$ kg/m^{2}s, $\Delta T_{sub,in} = 24.5$ °C, $\Delta T_w = 350$ °C.

References

[1] L.A. Bromley, Heat transfer in stable film boiling, Chem. Eng. Progress 46 (1950) 221–227.
[2] E.M. Sparrow, R.D. Cess, The effect of subcooled liquid on laminar film boiling, ASME J. Heat Transfer 84 (1962) 139–152.
[3] J.C.J. Koh, Analysis of film boiling on vertical surfaces, ASME J. Heat Transfer 84 (1) (1962) 55–62.

[4] K. Nishikawa, T. Ito, Two-phase boundary layer treatment of film boiling, Int. J. Heat Mass Transfer 9 (1966) 103–115.
[5] V.K. Dhir, G.P. Purohit, Subcooled film boiling heat transfer from spheres, Nuclear Eng. Des. 47 (1) (1978) 49–66.
[6] E.M. Greitzer, F.H. Abernathy, Film boiling on vertical surfaces, Int. J. Heat Mass Transfer 15 (1972) 475–491.
[7] T.D. Bui, V.K. Dhir, Film boiling on a vertical plate, ASME J. Heat Transfer 107 (1985) 756–763.
[8] R. Vijaykumar, V.K. Dhir, An experimental study of subcooled film boiling on a vertical surface-thermal aspects, ASME J. Heat Transfer 114 (1992) 169–178.
[9] T.D. Bui, Film and transition boiling of water on vertical surfaces, PhD thesis, University of California, Los Angeles, CA, 1984.
[10] M. Shiotsu, K. Hama, Film boiling heat transfer from a vertical cylinder in forced flow of liquids under saturated and subcooled conditions at pressures, Nuclear Eng. Des. 200 (2000) 23–38.
[11] Y.Y. Hsu, J.W. Westwater, Approximate theory for film boiling on vertical surfaces, Chem. Eng. Progress Sympos. Ser. 56 (30) (1960) 15–24.
[12] G.E. Coury, A.E. Duckler, Turbulent film boiling on vertical surfaces. A study including the influence of interfacial waves, Proceedings of International Heat Transfer Conference, Paris, Paper No. B.3.6, 1970.
[13] N.V. Suryanarayana, H.Jr. Merte, Film boiling on vertical surfaces, ASME J. Heat Transfer 94 (1972) 371–384.
[14] M. Aritomi, A. Inoue, S. Aoki, K. Hanawa, Thermo-hydraulic behavior of inverted annular flow, Nuclear Eng. Des. 120 (1990) 281–291.
[15] P.K. Meduri, Wall heat flux partitioning during subcooled flow film boiling of water on a vertical surface, PhD thesis, University of California, Los Angeles, CA, 2007.
[16] N. Hammouda, D.C. Groeneveld, S.C. Cheng, Two-fluid modelling of inverted annular film boiling, Int. J. Heat Mass Transfer 40 (11) (1996) 2655–2670.
[17] N.I. Kolev, Film boiling on vertical plates and spheres, Exp. Thermal Fluid Sci. 18 (1998) 97–115.
[18] M. Mosaad, K. Johannsen, Experimental study of steady state film boiling heat transfer of subcooled water flowing upwards in a vertical tube, Exp. Thermal Fluid Sci. 2 (1989) 477–493.
[19] H. Ohtake, S. Nishio, Natural-convection film boiling heat transfer (experiments of subcooled film boiling with long vapor film), JSME Int. J. Ser. B 37 (1) (1994).
[20] J.J. Carbajo, A study on the rewetting temperature, Nuclear Eng. Des. 84 (1985) 21–52.
[21] M. Drucker, V.K. Dhir, Effects of high temperature and flow blockage on the reflood behavior of a 4-rod bundle, EPRI Report, NP-2122, 1981.
[22] S.C. Cheng, P.W.K. Lau, K.T. Poon, Measurements of true quench temperature of subcooled water under forced convective conditions, Int. J. Heat Mass Transfer 28 (1) (1985) 235–243.
[23] V.B. Khabenskii, V.S. Granovskii, A.A. Malakhov, Minimum wall superheat in film boiling with subheating, Inzhenerno-Fizicheskii Zhurnal 42 (3) (1982) 383–386.
[24] K. Adham-Khodaparast, J.J. Xu, M. Kawaji, Flow film boiling collapse and surface rewetting in normal and reduced gravity conditions, Int. J. Heat Mass Transfer 38 (15) (1995) 2749–2760.
[25] A. Sakurai, M. Shiotsu, K. Hata, Effect of system pressure on minimum film boiling temperature for various liquids, Exp. Thermal Fluid Sci. 3 (1990) 450–457.
[26] J. Sinha, L.E. Hochreiter, F.B. Cheung, Effects of surface roughness, oxidation level and liquid subcooling on the minimum film boiling temperature, Exp. Heat Transfer 16 (2003) 45–60.